Hydrothermal growth of single crystals of the quantum magnets: Clinoatacamite, paratacamite, and herbertsmithite

Shaoyan Chu,[1,a)] Peter Müller,[2] Daniel G. Nocera,[2] and Young S. Lee[3]
[1]*Center for Materials Science and Engineering, Massachusetts Institute of Technology, Cambridge, Massachusetts 02139, USA*
[2]*Department of Chemistry, Massachusetts Institute of Technology, Cambridge, Massachusetts 02139, USA*
[3]*Department of Physics, Massachusetts Institute of Technology, Cambridge, Massachusetts 02139, USA*

(Received 24 January 2011; accepted 14 February 2011; published online 3 March 2011)

We present a hydrothermal method for growing millimeter-sized crystals of the quantum magnets with formula $Cu_{4-x}Zn_x(OH)_6Cl_2$: clinoatacamite ($x=0$), paratacamite ($0.33<x<1$) and herbertsmithite ($x=1$). These highly pure single crystals have been characterized by x-ray diffraction, chemical analysis, Raman spectroscopy, and magnetic susceptibility measurements. This synthesis success opens the door for detailed investigations of the magnetic ground-state properties of these compounds. © *2011 American Institute of Physics*. [doi:10.1063/1.3562010]

Clinoatamite,[1] paratacamite,[2] and herbertsmithite[3] are related to the atacamite family of compounds of the general formula $Cu_{4-x}Zn_x(OH)_6Cl_2$. These materials have generated much recent excitement in the condensed matter physics community, as they are excellent candidates for research on the effects of frustration in quantum magnets.[4,5] The presence of kagomé lattice planes (a network of corner-sharing triangles) formed by the Cu ions in these compounds provide a promising framework to explore exotic ground states such as the quantum spin liquid. Recently, Nocera and co-workers[6] prepared microcrystalline polymorphs of $Cu_{4-x}Zn_x(OH)_6Cl_2$ by the treatment of malachite, $Cu_2(OH)_2CO_3$, with NaCl and HBF_4 under hydrothermal conditions. Since then, both synthetic and natural samples have been used for investigating the structure and properties of the materials.[7–12] Though there exist natural crystals that are about 1 mm in size, current research suffers from a lack of larger synthetic crystals. Due to their limited purity and size, natural mineral samples may not meet requirements for crucial experiments such as magnetic anisotropy measurements and neutron scattering. Growth of large crystals is critical to further progress in investigating these fascinating materials.

Synthesis of the atacamite family of compounds was undertaken over a few decades ago.[13] The challenge in growing the atacamite family members arises from tiny differences in the free energy between various products in the synthesis process.[14] In the naturally found minerals, the members of the atacamite family always occur together. Depending on the occupation number of zinc in the crystal lattice, there are several different species in the $Cu_{4-x}Zn_x(OH)_6Cl_2$ family. For $x<0.3$, the crystal symmetry is orthorhombic (atacamite) or monoclinic (botallackite and clinoatacamite). At $x>0.3$, the crystal symmetry increases to rhombohedral. This high symmetry phase with intermediate Zn occupancy ($0.33<x<1$) is zinc-containing paratacamite. The compositional end members at $x=1$ are known as polymorphs of herbertsmithite and kapellasite.[15] In this report, we describe crystal growth technology and characterizations of clinoatacamite, paratacamite, and herbertsmithite. Hydrothermal growth experiments were performed by using a three-zone furnace. Typical starting materials and growth temperatures for the three compounds that are the subject of this study are listed in Table I. The formation of the compounds likely proceeds according to the following reactions: $(4-x)CuO + ZnCl_2 + 3H_2O \rightarrow Cu_{4-x}Zn_x(OH)_6Cl_2 + (1-x)ZnO$ or $(4-x)Cu(OH)_2 + ZnCl_2 \rightarrow Cu_{4-x}Zn_x(OH)_6Cl_2 + (1-x)ZnO + (1-x)H_2O$.

By varying the ratio of the starting materials and the reaction temperature, the value of x can be adjusted from 0 to 1 in the end product. High purity starting materials were combined with the desired composition ratios, and the mixture was sealed in a reaction cell (quartz tube) with a fill factor of ~85% after purging of air. The cell was then heated to ~190 °C and dwelled for two days to form microcrystalline powder of almost single. After this pre-reaction, the cell was held upright until the green-blue powder product deposited at one end. Then, the cell was again laid horizontally near the center of the three-zone furnace and slowly heated (2 °C/min) to the growth temperature. A temperature gradient at the cool end of the cell, where the crystals nucleated and grew, was controlled to ~0.1–0.5 °C/cm. Growth of the large crystals occurs as a re-crystallization process with the microcrystalline powder at the hot end as the source.

Photographs of the as-grown crystals of clinoatacamite, paratacamite, and herbertsmithite are presented in Fig. 1. The crystals usually grow in aggregated clusters. Large flattened crystals have a dark green-blue color with light green-blue streaks. The color of crystals obtained from different batches depends on the concentration of zinc in the products. Light blue crystals normally have higher concentrations of zinc. In agreement with natural minerals, the single crystals exhibit a hexahedral shape. The dominant growth direction is normal to the {101} plane for paratacamite and herbertsmithite and the {011} plane for clinoatacamite. As-grown crystals are easily cleaned with water in an ultrasonic cleaner and disaggregated by gentle crushing.

We used x-ray diffraction (XRD) (powder and single crystal) to determine the structure of these three synthetic species. The stoichiometric ratio of Cu/Zn was tested by inductively coupled plasma with atomic emission spectroscopy obtained by a Hololab 5000R Raman spectrometer. A super-

a)Electronic mail: sc79@mit.edu.

TABLE I. Structure and synthesis conditions of crystals of clinoatacamite, paratacamite, and herbertsmithite.

	Clinoatacamite	Paratacamite	Herbertsmithite
Composition	x=0	x=0.34±0.01	x=0.97±0.03
Starting materials (g)	CuO=2.0 g	$Cu(OH)_2$=0.20 g	CuO=0.172 g
	$CuCl_2 \cdot 2H_2O$=16.0 g	$CuCl_2$=0.20 g	$ZnCl_2$=4.0 g
	H_2O=16.0 g	$ZnCl_2$=2.0 g	ZnO=0.50 g
		H_2O=10.0 g	H_2O=4.0 g
Reaction cell [outside diameter, inner diameter, length (mm)]	16, 12, 260	12, 8, 270	12, 8, 191
Growth temperature [hot-end, cool-end, (°C)]	180, 176	175, 160	190,187
Crystal system	Monoclinic	Trigonal	Trigonal
Space group	$P2_1/n$	R-3	R-3m
a (Å)	6.1575(10)[a]	13.667(32)[b]	6.8447(6)[a]
b (Å)	6.8295(11)	13.667(32)	6.8447(6)
c (Å)	9.1144(14)	14.045(12)	14.116(3)
α(°)	90	90	90
β(°)	99.676(2)	90	90
γ(°)	90	120	120
Z	4	12	3
Magnetic transition temperatures (K)	14.0, 6.5, 6.2, 5.8	4.7	None above 1.8
Curie–Weiss temperature, θ (K)	−157	−221	−300
Curie constant, C (cm^3 K/mol Cu)	0.526	0.499	0.425

[a]Indicates the results obtained from single crystal XRD data at 100 K.
[b]Indicates the pulverized crystal's XRD data at 273 K.

conducting quantum interference device (SQUID) magnetometer (Quantum Design, MPMS) was employed to measure dc susceptibility at temperatures down to 1.8 K.

Clinoatacamite and paratacamite are classified in different crystal systems and space groups, but their XRD patterns are similar. A "fingerprint" on the powder XRD pattern for distinguishing paratacamite from clinoatacamite is appearance of diffraction peaks at a spacing of 28 nm>d >22 nm corresponding to $32° < 2\theta < 41°$ for Cu K_α radiation. As shown in Fig. 2, for paratacamite, there are two-peak and one-peak structures located at $2\theta \sim 32.5°$ and ~40°, respectively. In contrast, the diffraction pattern of clinoatacamite poses four-peak and two-peak structures near the same locations. This distinction is not removed by substituting zinc for copper in zinc-containing clinoatacamite. A reason for this is that the x-ray scattering factors for copper and zinc are similar. With this in mind, it is easy to understand why the powder XRD pattern of paratacamite is almost the same as that of herbertsmithite. Attempts at refining the zinc/copper ratio using XRD on both powder and single crystals of these two compounds proved difficult, as expected. The XRD refinement yields x with large uncertainty, where ICP-AES is used as a consistency check. Experimentally, it is impossible to distinguish paratacamite and herbertsmithite with standard powder XRD alone.

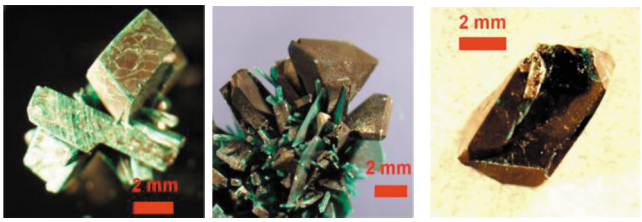

FIG. 1. (Color online) Morphology of as-grown crystals of clinoatacamite (left), paratacamite (middle), and herbertsmithite (right).

The chemical structures of these compounds can be further characterized by Raman scattering as shown in Fig. 3. When an unpolarized incident beam was perpendicular to the (011) plane of clinoatacamite and (101) plane of paratacamite or herbertsmithite, we observed 12 phonon modes for clinoatacamite and seven phonon modes for herbertsmithite within a Raman shift region from 100 to 1000 cm^{-1}. All of these peaks are in good agreement with those found in primary reports on natural and synthetic minerals.[14,16] However, not much has been previously reported on the differences between paratacamite (x<1) and herbertsmithite by Raman spectroscopy. It is quite clear that as the concentration of

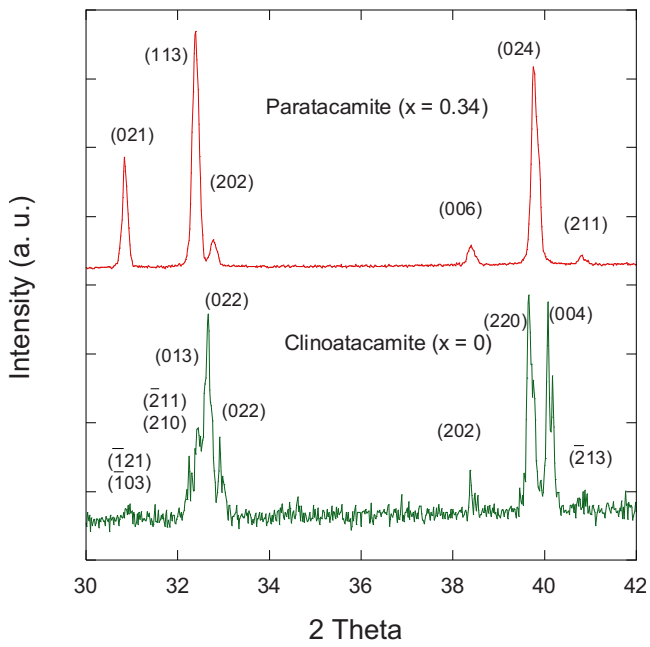

FIG. 2. (Color online) Partial powder XRD patterns for paratacamite (x=0.34) and clinoatacamite (x=0) with Cu K_α radiation.

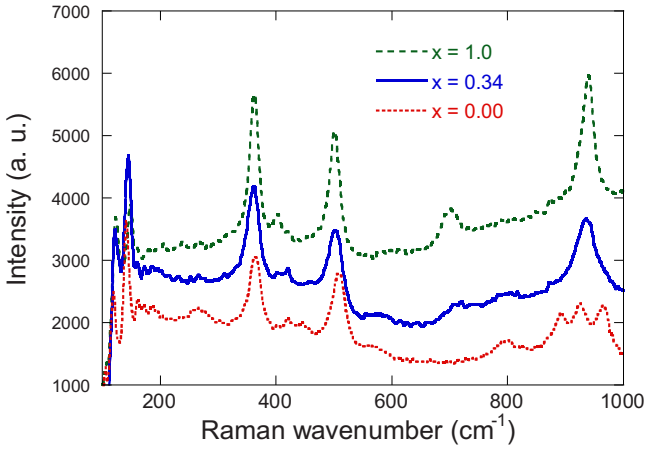

FIG. 3. (Color online) Raman spectra for the crystals of $Cu_{4-x}Zn_x(OH)_6Cl_2$, clinoatacamite (x=0), paratacamite (x=0.34), and herbertsmithite (x=1), measured with λ=785 nm excitation line.

zinc increases, a three-band structure at wavenumbers of 891.7, 924.4, and 964.4 cm^{-1} for clinoatacamite gradually merge into a single-band structure at 940.0 cm^{-1} for herbertsmithite. Meanwhile, the increase in zinc concentration enhances (reduces) the intensity of a band at around λ^{-1} ~700 cm^{-1} (~800 cm^{-1}). Five common phonon modes for these compounds correspond to Raman bands at wave numbers of ~120, ~145, ~360, ~505, and ~935 cm^{-1}.

The synthetic crystals have been used to examine a theoretical prediction that strong geometrical frustration in spin systems may suppress any magnetic long-range ordering (LRO) down to very low temperatures. Significant differences in the magnetic susceptibilities (χ=M/H) for these three compounds are shown in Fig. 4. A sharp change in the temperature dependence of χ generally indicates the occurrence of a magnetic phase transition. On cooling, clinoatacamite undergoes multiple transitions, indicated by kinks in the susceptibility. In contrast, paratacamite (x=0.34) has only one transition involving a frustrated antiferromagnetic phase with weak ferromagnetism. However, there is no definable magnetic LRO temperature for the herbertsmithite crystals down to the lowest measured temperature of 1.8 K. Since the magnetic susceptibility measurements using a SQUID probe the bulk magnetization of the sample, a single magnetic transition (or the lack thereof) for synthetic paratacamite (herbertsmithite) indicates that our crystals are free of inclusion of any other family members with lower lattice symmetry.

At high temperature, all three compounds display paramagnetic behavior and the temperature dependence of their susceptibility obeys the Curie–Weiss law, χ=C/(T−θ). The fitted Curie–Weiss temperature, θ, and Curie constant, C, are listed in Table I. A significant magnetic anisotropy (not shown here) for the single crystal of paratacamite (x=0.34) is observed. This anisotropy changes with temperature and has a field-dependent behavior. Detailed studies of the anisotropy of the Cu^{2+} moments and of the magnetic phases in

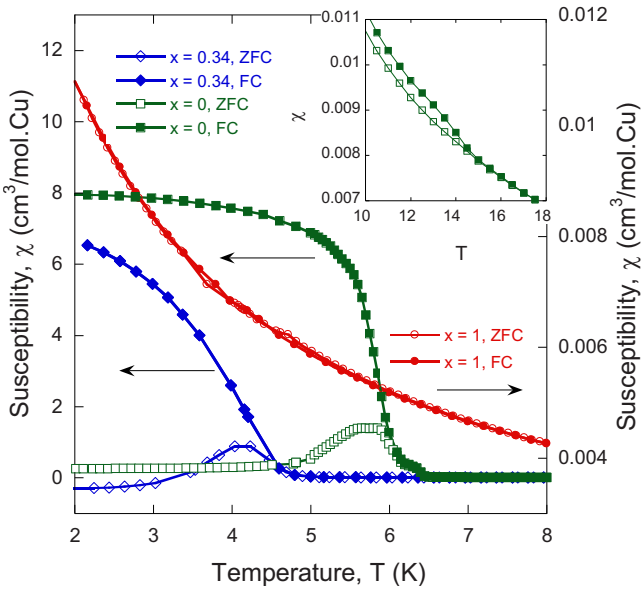

FIG. 4. (Color online) Temperature dependence of dc susceptibility for clinoatacamite (x=0), paratacamite (x=0.34) and herbertsmithite (x=1) in the field of 20 Oe with random orientation. ZFC and FC notes zero-field-cool and field-cool measurement modes. Inset: separation of ZFC and FC indicates a magnetic phase transition of clinoatacamite (x=0) at T~14 K.

these kagomé systems are topics of future work.

The authors acknowledge helpful discussions with Tianheng Han and Patrick Lee. This work was supported by the Department of Energy under Grant No. DE-FG02-04ER46134. This work used facilities supported by the MRSEC Program of the NSF under Award No. DMR 0819762.

[1]J. D. Grice, J. T. Szymanski, and J. L. Jambor, Can. Mineral. **34**, 73 (1996).
[2]M. E. Fleet, Acta Crystallogr., Sect. B: Struct. Crystallogr. Cryst. Chem. **31**, 183 (1975).
[3]R. S. W. Braithwaite, K. Mereiter, W. H. Paar, and A. M. Clark, Miner. Mag. **68**, 527 (2004).
[4]B. G. Levi, Phys. Today **60**, 16 (2007).
[5]W.-H. Ko, P. A. Lee, and X.-G. Wen, Phys. Rev. B **79**, 214502 (2009).
[6]M. P. Shores, E. A. Nytko, B. M. Bartlett, and D. G. Nocera, J. Am. Chem. Soc. **127**, 13462 (2005).
[7]J. S. Helton, K. Matan, M. P. Shores, E. A. Nytko, B. M. Bartett, Y. Yoshida, Y. Takano, Y. Qiu, J.-H. Chung, D. G. Nocera, and Y. S. Lee, Phys. Rev. Lett. **98**, 107204 (2007).
[8]S.-H. Lee, H. Kikuchi, Y. Qiu, B. Lake, Q. Huang, K. Habicht, and K. Kiefer, Nature Mater. **6**, 853 (2007).
[9]X.-G. Zheng and K. Nishiyama, Physica B **374–375**, 156 (2006).
[10]X. G. Zheng, T. Kawae, Y. Kashitani, C. S. Li, N. Tateiwa, K. Takeda, H. Yamada, C. N. Xu, and Y. Ren, Phys. Rev. B **71**, 052409 (2005).
[11]X. G. Zheng, H. Kubozono, K. Nishiyama, W. Higemoto, T. Kawae, A. Koda, and C. N. Xu, Phys. Rev. Lett. **95**, 057201 (2005).
[12]A. S. Wills, T. G. Perring, S. Raymond, B. Fak, J.-Y. Henry, and M. Telling, J. Phys.: Condens. Matter **145**, 012056 (2009).
[13]A. M. Pollard, R. G. Thomas, and P. A. Williams, Miner. Mag. **53**, 557 (1989).
[14]R. L. Frost, Spectrochim. Acta, Part A **59**, 1195 (2003).
[15]W. Krause, H.-J. Bernhardt, R. S. W. Braithwaite, U. Kolitsch, and R. Pritchard, Miner. Mag. **70**, 329 (2006).
[16]W. Martens, R. L. Frost, and P. A. Williams, Neues Jahrb. Mineral., Abh. **178**, 197 (2003).